Polymer Testing 137 (2024) 108520

Contents lists available at ScienceDirect

Polymer Testing

journal homepage: www.elsevier.com/locate/polytest

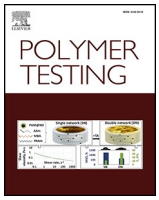

A novel method for determining the pressure dependent characteristics of polymer melt during micro injection molding

Junjie Liu [a], Baishun Zhao [a], Dimitrios Kontziampasis [b,c,d], Bingyan Jiang [a], Wangqing Wu [a,c,*]

[a] State Key Laboratory of Precision Manufacturing for Extreme Service Performance, School of Mechanical and Electrical Engineering, Central South University, 410083, Changsha, China
[b] Department of Mechanical and Industrial Engineering, School of Science and Engineering, University of Dundee, DD1 4HN, Dundee, Scotland, UK
[c] Dundee International Institute of Central South University, Central South University, 410083, Changsha, China
[d] School of Mechanical Engineering, Faculty of Science and Engineering, The University of Leeds, Leeds, Yorkshire, LS2 9JT, UK

ARTICLE INFO

Keywords:
Micro injection molding
Simulation
Cross-WLF model
Polymer

ABSTRACT

Micro injection molding is used to manufacture thin-walled parts with micron-scale structures. wherein high shear rate and high injection pressure process conditions appear. Consequently, the pressure dependence of polymer melt viscosity at the microscale cannot be ignored. However, in the simulation analysis of the micro-injection molding process, almost all the Cross-WLF models of polymeric materials are omitting the pressure dependence parameter D_3. This has a huge impact on the accuracy of the simulation results. Herein, a method that combines experimental characterization and filling simulation is proposed for the determination of the pressure dependence of polymer melts during micro injection molding. D_3 in the Cross-WLF model of Polymethyl methacrylate (PMMA) and Cycloolefin copolymer (COC) is characterized by capillary rheometer and counter pressure chamber. The developed viscosity model including D_3 is used for a filling simulation and is compared with the experimental results. The model flow simulation results showcases that the prediction accuracy of the viscosity model is significantly improved after considering D_3. These results are of great significance, as they can be used to reduce the development cost and to improve the simulation accuracy of the micro injection molding filling process.

1. Introduction

In modern scientific literature the technology of micro injection molding technology plays an important role in applications that span in numerous fields, some of which are optoelectronic communications [1–3], biochemical medicine [4–7], and precision machinery [8–10]. Micro injection molding is now the main method to achieve low-cost mass manufacturing of polymer microparts. It not only can produce polymer microfabricated parts with high efficiency [11,12], but also ensure that the produced microparts have high consistency in accuracy, shape and size.

Contrary to the working conditions of the traditional injection molding method, the cross-scale molding of micro injection molding parts employ the use of small size features size in conjunction with an increased specific surface area, leading to the appearance of micro-scale effects, [13–15]. Additionally, in micro injection molding large shear rate [16–18] and large injection pressure conditions exist [19,20], which increases the development cost of micro injection molds. In order to ensure the quality of molded parts, a filling simulation of molded parts is typically employed in the development stage, using CAE mold flow analysis, as a means to reduce manufacturing costs [21]. Another characteristic of the method is that the pressure dependence of the polymer melt is not negligible at high injection or cavity pressures [22]. However, in most of the existing CAE filling simulations published in literature, the pressure dependence of the polymer melt is not taken into consideration in the viscosity model. This translates to the simulation results failing to accurately and truly predict the defects that exist in the parts, corresponding to a great increase in the cost of mold development.

Cross-WLF model [23,24] is the favorite polymer viscosity model from mainstream injection molding CAE mold flow analysis software. This model is a viscosity equation that contains seven parameters, which are used to describe the flow behavior of polymer melts. This model has

* Corresponding author. State Key Laboratory of Precision Manufacturing for Extreme Service Performance, School of Mechanical and Electrical Engineering, Central South University, 410083, Changsha, China.
E-mail address: csuwwq@csu.edu.cn (W. Wu).

https://doi.org/10.1016/j.polymertesting.2024.108520
Received 22 May 2024; Received in revised form 8 July 2024; Accepted 15 July 2024
Available online 15 July 2024

Table 1
Material properties of PMMA.

Item	Rating	Unit	Test method
Melt Flow Index	2	cm^3/10min	ISO 1133
Solid density	1.19	g/cm^3	ISO 1183
Vicat Softening Temperature	115	°C	ISO 306/B120
Water absorption rate	0.3	%	ISO 62
Glass transition temperature	105	°C	ISO 178
Heat deflection temperature	84	°C	ISO 75-2
Number-average Molecular Weight	50	kg/mol	GPC
Weight-average Molecular Weight	81	kg/mol	GPC

Table 2
Material properties of COC.

Item	Rating	Unit	Test method
Melt Flow Index	48	cm^3/10min	ISO 1133
Solid density	1.02	g/cm^3	ISO 1183
Vicat Softening Temperature	133	°C	ISO 306/B120
Water absorption rate	0.01	%	ISO 62
Glass transition temperature	134	°C	ISO 178
Heat deflection temperature	127	°C	ISO 75-2/B
Number-average Molecular Weight	31.2	kg/mol	GPC
Weight-average Molecular Weight	76.4	kg/mol	GPC

Table 3
Grid parameters and boundary conditions of simulation model.

Slit thickness h	Mesh type	Model scale	Bundary conditions	Msh quantity
0.35 mm	Tetrahedral element	1:1 molded parts	Consistent with the experiments	3864396
0.5 mm	Tetrahedral element	1:1 molded parts	Consistent with the experiments	1760072

a high degree of complexity and can fully describe the effects of shear rate, temperature, pressure, as well as other factors on the shear viscosity during the filling process. The pressure dependence parameter D_3 in the seven-parameter model, is used to describe the pressure dependence of polymer melt viscosity. However, one can notice that in the material library of numerous CAE software, there are only but a few materials that have complete datasets of D_3, and for this reason the D_3 of most materials is set to 0 by default. This fact appears to have a minor effect on ordinary injection molding filling simulations, but for micro injection molding with high shear rate and high injection pressure, D_3 cannot be ignored. However, literature shows that the measurement and the calculation of D_3 is not standardized in the filling simulation based on micro injection molding technology.

There is a big number of research carried out in literature that is revolving around the pressure dependence of polymer melt viscosity during micro injection molding. Tomas et al. [25] studied the temperature and pressure sensitivity of seven types of polymeric materials, showing that those who demonstrated high pressure sensitivity also have increased sensitivity to temperature and vice versa. Dietmar et al. [26] proposed the use of a capillary rheometer and a counter pressure chamber to study the influence of uncorrected pressure on the viscosity of polymer melt. The results showed that the calculation error of viscosity was caused by ignoring the influence of pressure, and that it was approximately 12%–14 %. Others [27] investigated the effect of pressure on the rheological properties of polymer extrusion using a parallel plate rheometer and a capillary rheometer, where the K-BKZ model fitted by the experimental data corresponded well to the effects of pressure and temperature on the steady-state shear viscosity and the transient tensile viscosity, while also modeling the inlet pressure drop of the polymer appropriately.

In another study [28] a capillary rheometer and a counter pressure chamber were employed to measure the pressure influence coefficients β_δ and β_γ of different polymers based on the Barus equation under constant shear velocity and constant shear stress, proving a $\beta_\gamma = n\beta_\delta$ relationship when the shear rate is in the power law region. This relationship was validated also from different [29–31], which studied the pressure dependence coefficient of polymer melts. Volpe et al. [32] used a modified slit rheometer and an injection molding apparatus to calculate the pressure dependence parameter in the Cross-Vogel five-parameter model for injection molding, with results showing good fitting of experimental and predicted values. There is also research that calculated D_3 of the Cross-WLF viscosity model in the zero shear viscosity region, via the use of a capillary rheometer and a counter pressure chamber. There, they employed tailored molds to measure the pressure during the injection process, achieving results, which prove that a pressure profile obtained from Moldflow simulation with the addition of D_3 was even closer to the experimental results [33,34]. Additionally, they established a proxy model that is based on the pressure dependence, where the measured D_3 is used for reducing the pressure prediction error of the simulation.

The above mentioned studies showcase clearly that numerous problems still exist in the current research literature regarding pressure dependence parameter measurements. Most of the studies are focused on the pressure influence coefficient in the Barus equation, which only reflects the pressure dependence of the polymer and cannot be directly used in the viscosity model of CAE filling simulation. In parallel, the shear rate range typically used for the study of the pressure dependence of a polymer is limited, and the test range is narrow, while it is not focused on the large shear rate conditions of the micro injection molding. Finally, most studies appear to be focused on the measurement of the pressure dependence parameter itself, whereas they have not been tested in actual working conditions.

Several scholars have studied the pressure dependence of crystalline and amorphous polymers [28,35,36]. From their studies, it can be found that the pressure dependence of most amorphous polymers is much larger than that of crystalline polymers. This pressure dependence is further amplified under micro-injection molding conditions. Therefore, two amorphous polymer materials with strong pressure dependence, which are commonly used in engineering, are selected for the study. In this work, two polymeric materials with strong pressure dependence, Polymethyl methacrylate (PMMA) and (Cycloolefin copolymer) COC, are tested at high shear rates (10^2-10^4 s^{-1}) using a high pressure capillary rheometer and a counter pressure chamber. The characterization of D_3 of the Cross-WLF seven-parameter model is performed in the non-Newtonian region (power-law region) of the two polymers, where the fitting of the remaining six parameters is performed. After obtaining the complete seven-parameter model, the simulation of the thin-walled part for mode flow analysis is established. The filling simulations of micro injection molding are performed with using commercial software (Moldflow), and subsequently are compared with micro injection molded that are built under the same process parameters.

2. Experimentation

2.1. Materials

The polymeric materials that are used for the experiments are pelletized PMMA (produced by ACRYREX® CM-205, Taiwan) and COC (produced by TOPAS®, TOPAS 5013-10L, Fuji, Japan). Their performance is shown in Table 1, Table 2. The PMMA material is stored and dried in a dryer at 80 °C for 8 h, while COC is dried in a dryer at 100 °C for 8 h. Both materials are used immediately after drying so that there is no effect from moisture in the environment to the process.

2.2. Pressure dependence parameter calculation model

The Williams-Landel-Ferry (WLF) model is used to predict the effect

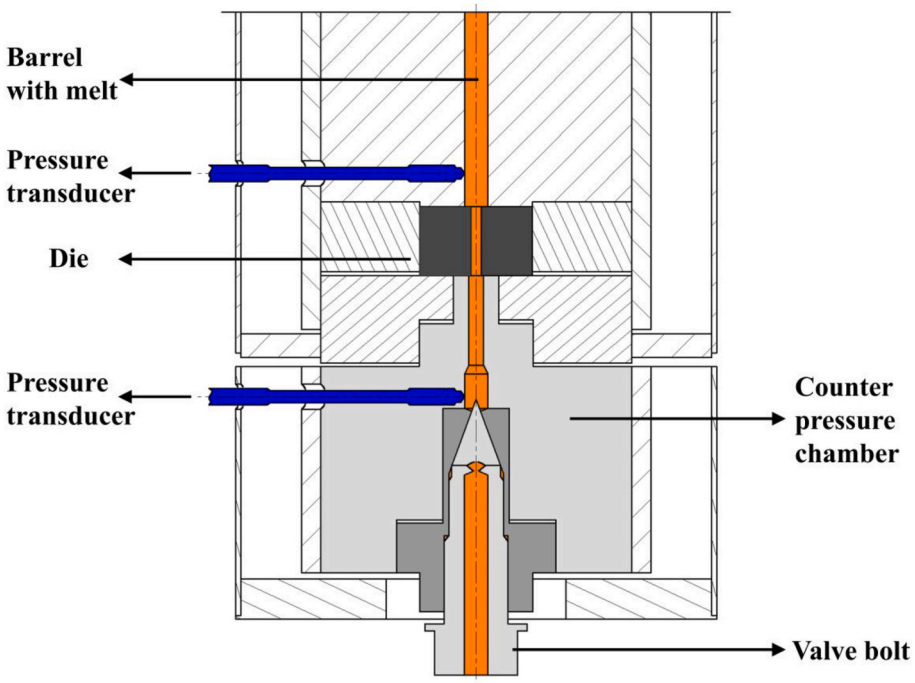

Fig. 1. Counter pressure chamber assembly fitted below the Rheometer die.

of temperature on the viscosity of amorphous polymer melts in the general form:

$$\eta_0(T) = D_1 \exp\left[\frac{-A_1(T-T^*)}{A_2+(T-T^*)}\right] \tag{1}$$

where $\eta_0(T)$ is the zero shear viscosity at temperature T, the glass transition temperature is T^*, and D_1, A_1, A_2 are the fitted data parameters.

In the micro injection molding process, injection pressures exceeding 80 MPa are common, so the WLF equation needs to be corrected for the reduction in free volume due to pressure. This correction is expressed in the parameter T^*, whose linear relationship with pressure is given by:

$$T^* = D_2 + D_3 \cdot P \tag{2}$$

where D_2 is the model fit coefficient, and D_3 is the pressure dependence parameter in respect to the pressure P. By associating Eq. (1) and Eq. (2), the zero shear viscosity at any temperature and pressure is obtained:

$$\eta_0(T,P) = D_1 \exp\left[\frac{-A_1(T-D_2-D_3P)}{\widetilde{A_2}+T-D_2}\right] \tag{3}$$

where:

$$\widetilde{A_2} = A_2 - D_3P \tag{4}$$

For polymer melts with shear thinning phenomena, the Cross equation is employed, in order to describe the dependence of polymer melt viscosity on the shear rate after determining the zero-shear viscosity at temperature T and pressure P. The Cross model was used to describe the dependence of polymer melt viscosity on shear rate. The Cross-WLF is obtained by associating the Cross model with the WLF equations and is expressed as follows:

$$\eta(\dot{\gamma},T,P) = \frac{\eta_0(T,P)}{1+\left(\frac{\eta_0(T,P)}{\tau^*}\cdot\dot{\gamma}\right)^{1-n}} \tag{5}$$

where τ^* denotes the critical stress level at the transition to shear thinning, as determined by the curve fitting, n is the power-law exponent in the method denoting high shear rate, and $\dot{\gamma}$ denotes the shear rate.

Eq. (3), can be rewritten as:

$$\eta_0(T,P) = D_1 \cdot \mathrm{e}^{\left[\frac{-A_1(T-D_2)}{\widetilde{A_2}+T-D_2}\right]} \cdot e^{\theta \cdot P} \tag{6}$$

where the equivalent pressure dependence parameter θ is:

$$\theta = \frac{A_1 D_3}{\widetilde{A_2}+T-D_2} \tag{7}$$

From Eq. (7), D_3 can be resulted by an experiment that yields the parameter θ, when the parameters A_1, $\widetilde{A_2}$, D_2 are known.

The Poiseuille equation is used to measure the viscosity of a polymer melt that is flowing through a capillary orifice mold under a certain pressure gradient. For a Newtonian fluid, it is expressed as:

$$\Delta P = \eta \cdot \gamma \cdot \frac{2L}{R} \tag{8}$$

where ΔP is the pressure difference between the inlet and the outlet of the capillary orifice mold, R is the capillary radius of the capillary orifice mold, L is the length of the orifice mold, and γ is the wall shear rate.

Taking into account the effect of pressure on viscosity into the Poiseuille equation, it becomes:

$$\frac{dP}{dL} = -\frac{2\eta \cdot e^{\theta P} \cdot \gamma}{R} \tag{9}$$

Including the effect of shear rate and pressure on viscosity in the Cross model into the Poiseuille equation, Eq. (9) can be rewritten as:

$$\frac{dP}{dL} = -\frac{2 \cdot \eta_0 \cdot e^{\theta P} \cdot \gamma}{R \cdot \left[1+\frac{\eta_0 \cdot e^{\theta P}}{\tau^*}\gamma\right]^{1-n}} \tag{10}$$

Due to the difficulty of solving Eq. (10) directly, it is necessary to use a reasonable equivalent. At high shear rates, the Cross model approximately overlaps with the power-law model, so the power-law model can be used for approximate calculations. At high shear rates ($\dot{\gamma} \gg \tau^*/\eta_0$), the Cross model reduces to a power-law model:

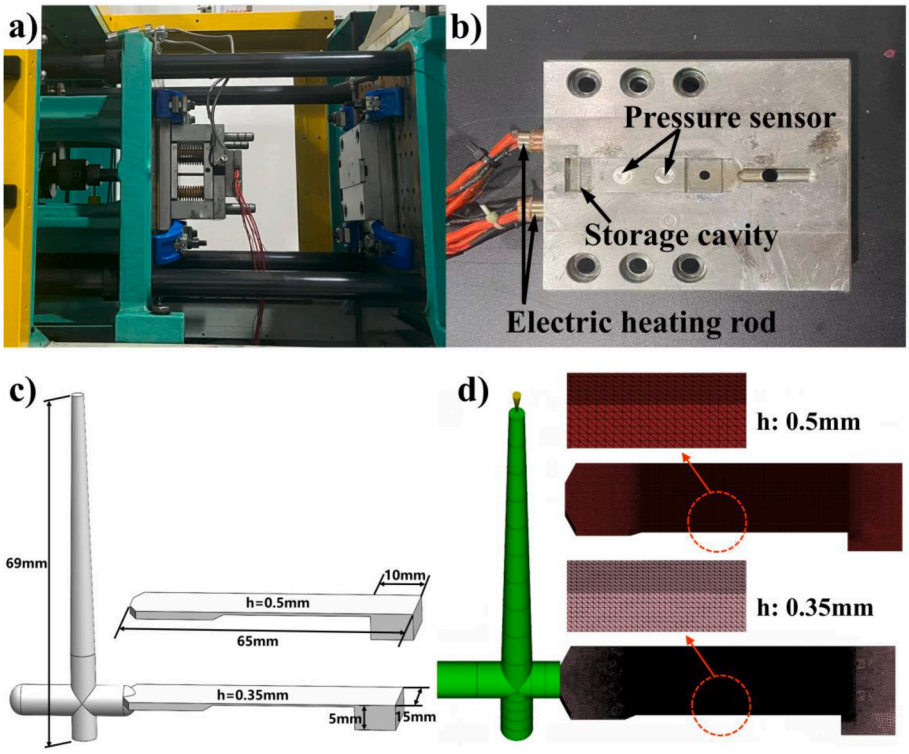

Fig. 2. Micro injection molding test mold. a) mold, b) mold core, c) 3D model of the manufactured part, d) simulation model in Moldflow.

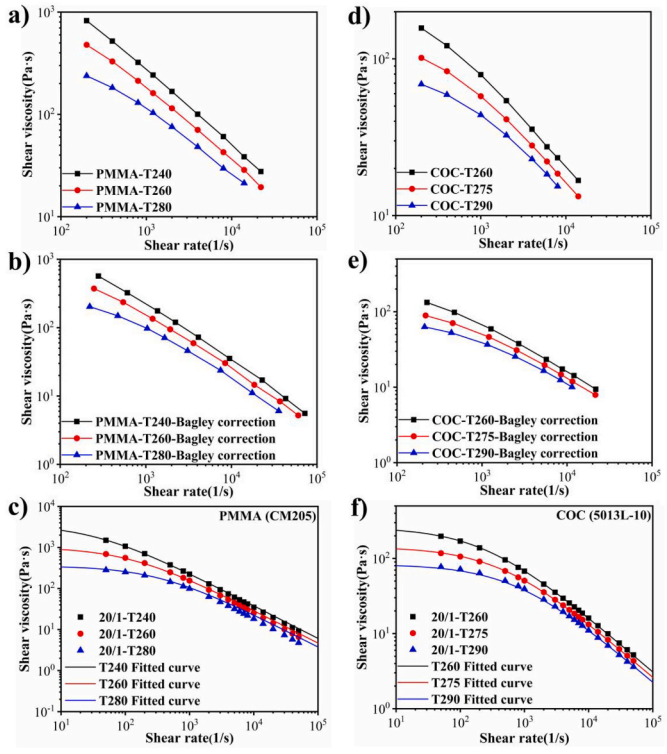

Fig. 3. Experimental results of PMMA, COC viscosity test. a) PMMA uncorrected viscosity, b) PMMA viscosity after Bagley correction, c) PMMA model fitting curve, d) COC uncorrected viscosity, e) COC viscosity after Bagley correction, f) COC model fitting curve.

$$\eta(\dot{\gamma}, P) = K \bullet \dot{\gamma}_p^{n-1} \bullet e^{n\theta P} \tag{11}$$

By substituting Eq. (11) into Eq. (9), and integrating in the direction of length L:

$$\eta = \frac{e^{-n\cdot\theta\cdot P_2} - e^{-n\cdot\theta\cdot P_1}}{n\cdot\theta\cdot\dot{\gamma}_p\cdot 2L}\cdot R \tag{12}$$

Using Eq. (11), the equivalent pressure dependence parameter θ can be derived after the viscosity in the power-law region is measured experimentally, allowing for D_3 to be obtained using a quadratic calculation.

2.3. Experimental equipment and methods

2.3.1. High pressure capillary rheometer and counter pressure chamber

Experimental measurements are carried out using a single-cylinder capillary rheometer (Rheograph 50; Goettfert, Germany) with a counter pressure chamber (Goettfert, Germany). The cylinder has Ø 15 mm, while the maximum temperature it can withstand is 500 °C, and the speed range of the plunger ranges from 0.00004 to 40 mm/s. The size of the selected die is 20/1/180 (length, diameter, entrance angle), as it needs to be used with a counter pressure chamber.

As shown in Fig. 1, the counter pressure chamber is positioned at the capillary die's exit, and a needle valve adjustment is used to create a positive pressure at the outlet. To guarantee that the shear rate is not affected when measuring in the constant velocity mode, the relevant inlet pressure is changed appropriately. For the purpose of short shot experiments, the experimental temperatures of PMMA and COC are selected according to the lowest processing melt temperature provided by the manufacturer. Therefore, every experiment for PMMA is conducted at 240 °C with shear rates ranging from 500 to 6000 s^{-1}, while every experiment for COC is conducted at 260 °C with shear rates ranging from 500 to 10000 s^{-1}. The entrance and exit pressures are recorded by two 2k bar pressure sensors.

Table 4
Six Cross-WLF model parameters obtained by curve fitting.

Parameter	PMMA (CM-205)	COC (5013L-10)
$n(-)$	0.2036	0.2646
τ^* (Pa)	1.19E+05	6.35E+04
D_1(Pa·s)	5.21E+18	6.90E+18
D_2(K)	377.15	343.15
$A_1(-)$	48.14	48.09
$\tilde{A}_2$(K)	51.6	51.6

2.3.2. Shear viscosity measurement

Viscosity measurements are performed with a single-cylinder capillary rheometer, which is subsequently used to fit the remaining six parameters of the Cross-WLF model, except D_3, employing the identical orifice sizes as previously stated before. Experiments for each material are carried out at three distinct temperatures, so as to ensure the accuracy of the fitted data. Viscosity measurements for PMMA are carried out at 240, 260, and 280 °C, with experimental shear rates ranging from 200 to 20000 s^{-1}, while for COC are carried out at 260, 275, and 290 °C, with shear rates ranging from 200 to 20000 s^{-1}.

2.3.3. Filling simulation

A filling simulation model of the thin-walled sections with a high width-to-thickness ratio is constructed, and its structure and parameters are depicted in Fig. 2. The injection molding simulation study was performed using Moldflow, in order to set the parameters of the Cross-WLF model in the filling simulation to those obtained by experimental fitting, and also to add the measurements of D_3. The simulation results obtained from the original Cross-WLF model in the software are then compared with the experimentally obtained simulation results of the model with the addition of D_3 (see Table 3).

2.3.4. Micro injection molding experiment

Micro injection molding experiments are carried out using a homemade mold and a special injection machine for precision parts (Arburg 370S), as can be seen in Fig. 2 (a, b). The thin-walled parts obtained from the experiments are compared with the simulation results. The parameters that are used in the experiments are identical to those used in the simulations.

3. Results and discussion

3.1. Shear viscosity characterization

As can be seen in Fig. 3, the viscosity of both PMMA and COC is temperature dependent and decreases significantly with the increase of temperature. When using a capillary rheometer to test the rheological properties of materials, the pressure sensor is positioned on the barrel wall rather than the capillary tube. Furthermore, when the material is squeezed into the capillary die from the cylinder, viscous friction is generated between the various flow layers. This is subsequently combined with the elastic deformation of the material, resulting in the pressure difference that is measured by the capillary inlet pressure sensor, which consists of the sum of the inlet, the fully developed zone, and the outlet pressure drops. As a result, It is necessary to induce corrections when calculating the pressure gradient, based on the pressure difference. It is important to note that during testing of non-Newtonian fluids, a wall slip phenomenon occurs within the capillary die, whereas if this is not corrected, leads to incorrect equations and resulting calculations [29,37].

In this work, a zero L/D die with an 1.0 mm diameter, and dimensions of 0/1/90 (length, diameter, and entrance angle) is selected in order to repeat the experiment under the same experimental conditions.

Table 5
Equivalent pressure dependence parameter θ and pressure dependence parameter D_3 for PMMA and COC.

Parameter	PMMA(CM205)	COC(5013L-10)
θ(1/bar)	0.005076	0.009165
D_3 (K/Pa)	1.98E-07	4.60E-07

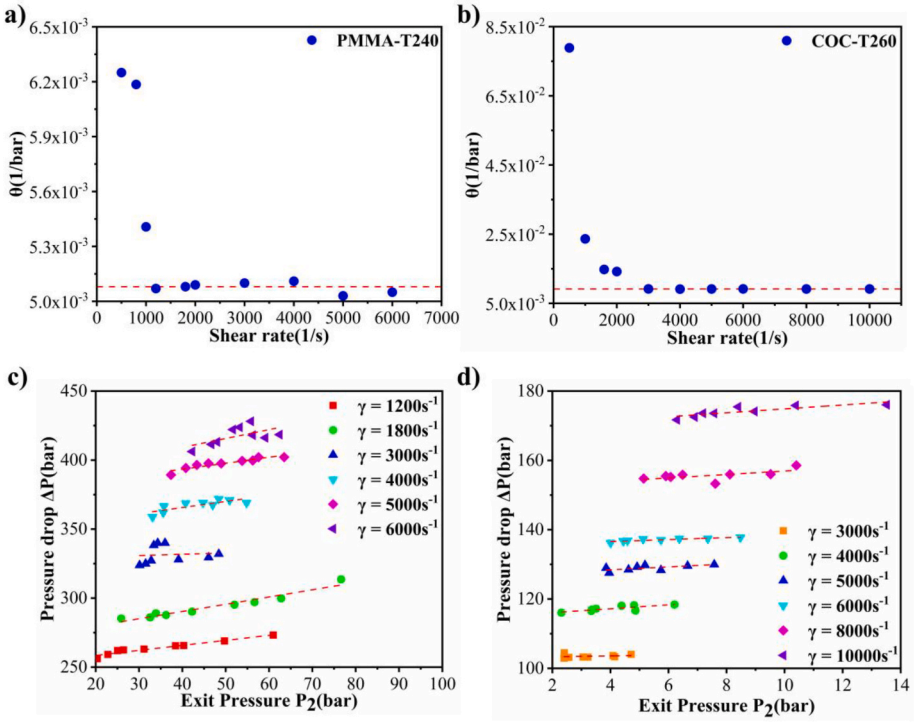

Fig. 4. The equivalent pressure dependence parameter θ for (a) PMMA, and (b) COC. The calculate relationship between outlet pressure and pressure drop for (c) PMMA, and (d) COC.

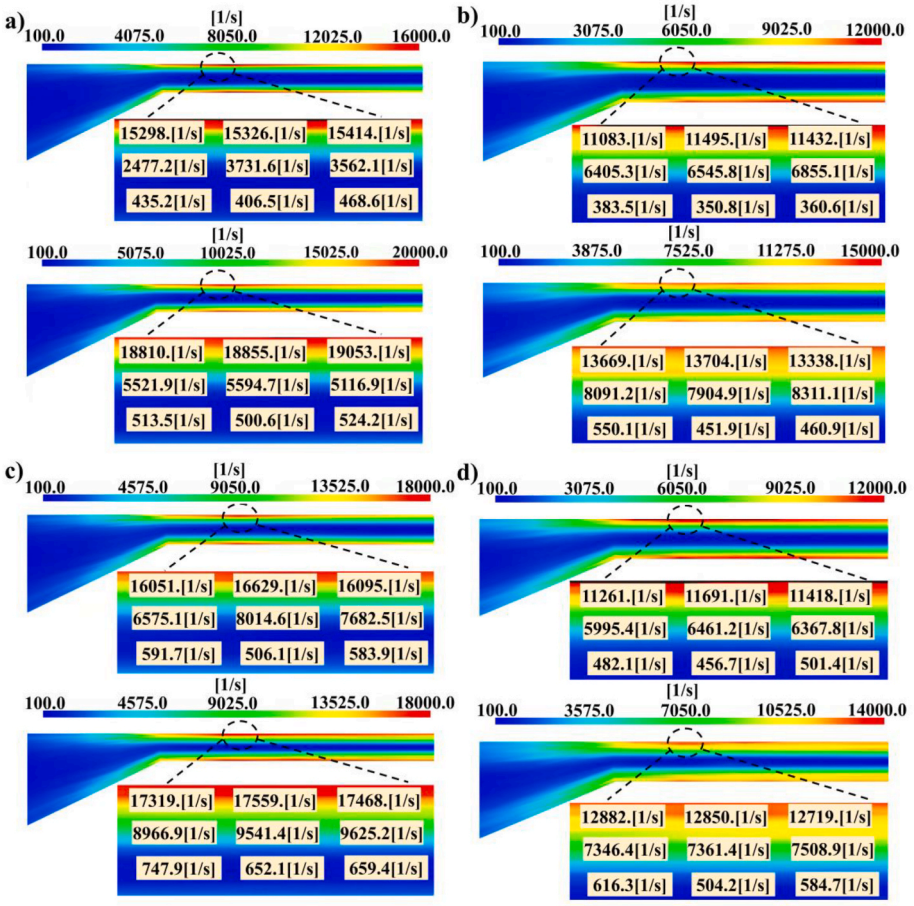

Fig. 5. Distribution of the shear rate in cross-section, as obtained from filling simulation of the 0.35 mm and the 0.5 mm thin-walled model. (a, b) PMMA, and (c, d) COC. It is important to note that the top half of each figure is the simulation result of a seven-parameter viscosity model with D_3, and the bottom half is without D_3.

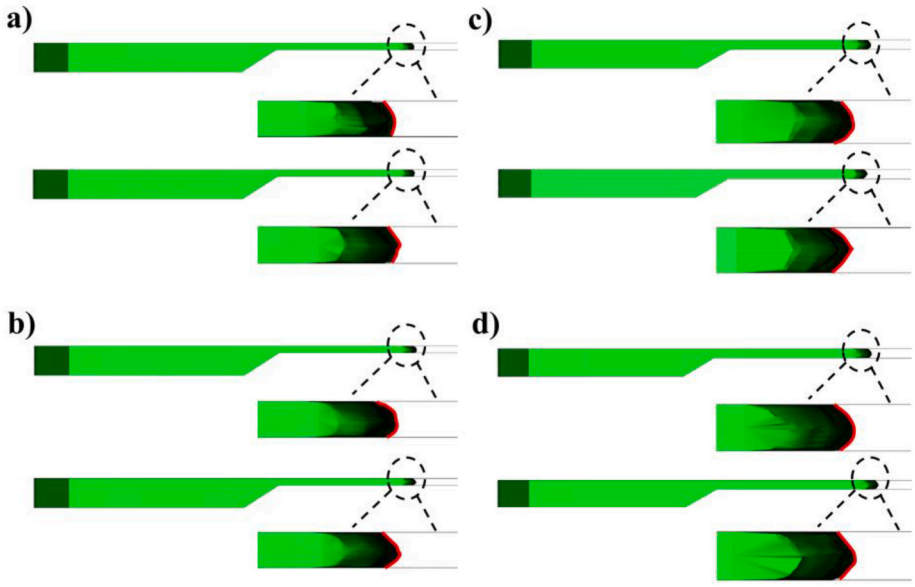

Fig. 6. Simulated flow fronts for 0.35 mm and 0.5 mm thin-walled model filling for COC (a, c) and PMMA (b, d). It is important to note that the top half of each figure is the simulation result of a seven-parameter viscosity model with D_3, and the bottom half is without D_3.

The viscosity data that is measured under the L/D = 20/1 die is corrected via the Bagley correction method. A Wessenberg-Rabinowitsch correction is also performed to eliminate the influence of wall slip [38]. After corrections, the viscosity data of PMMA and COC decreased at all three temperatures, but the overall trend remained the same as before (see Fig. 3). It can be seen from Fig. 3(b) and (e) that the thinning

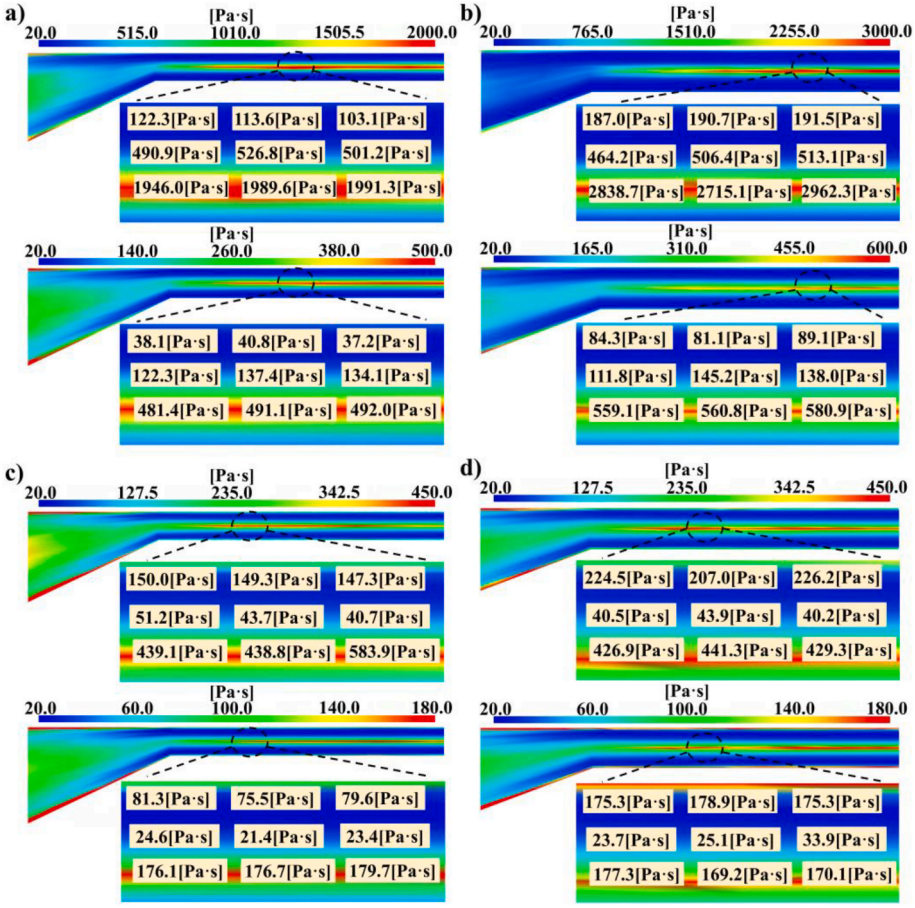

Fig. 7. Distribution of shear viscosity in cross-section obtained from filling simulation of the 0.35 mm and 0.5 mm thin-walled model for PMMA (a, b) and COC (c, d). It is important to note that the top half of each figure is the simulation result of a seven-parameter viscosity model with D_3, and the bottom half is without D_3.

of PMMA is more evident than that of COC. The hypothesis is that the phenomenon can be described using the molecular chain disentanglement mechanism. COC has a cyclic structure in its molecular chain, which is stiff, and therefore results in the increase of material hardness and young modulus, while PMMA is a linear polymer with methylester-based side chains. As the shear rate increases, due to the molecular chain of PMMA is linear, therefore its molecular chain is more likely to stretch and deform, which reduces the flow resistance. The ring structure of the COC molecular chain requires more energy to deform than the ordinary entanglement of the chain structure, resulting in greater flow resistance at the same shear rate.

The above mentioned algorithm is used to fit the six parameters of the Cross-WLF model of PMMA and COC, except D_3 (see Table 4). The fitted Cross-WLF model curves are drawn using each parameter from Table 1, as shown in Fig. 3(c) and (f). There PMMA curve is in the power-law region at shear rates larger than 500 s^{-1}, and COC curve is in the power-law area at shear rates more than 3000 s^{-1}.

3.2. Determination of the pressure dependence parameter

The outlet pressure P2 is increased by gradually tightening the rotary needle valve below the counter pressure chamber, and the tested shear rate is gradually increased until the polymer melt reaches the power-law region. The experiment records inlet and exit pressures at various needle valve angles and shear rates, which are then used in Eq. (13). In order to calculate θ. In Eq. (12), η_i represents the viscosity of the two polymers in the power-law region, and N represents the total number of the measured data points. To calculate the equivalent pressure dependence parameter θ at different shear rates, Eq. (13) is used. To calculate D_3 for PMMA (240 °C) and COC (260 °C), the six Cross-WLF parameters from Section 3.1 and Eq. (7) are combined:

$$\lambda^2 = \sum_i \left(\eta_i - \frac{\sum_i \eta_i}{N} \right)^2 \tag{13}$$

The equivalent pressure dependence parameter of the two polymers decreases in reverse analogous fashion comparing to the shear rate under the measurement conditions of the constant shear rate mode of the capillary rheometer, in agreement to Ruth et al. [28] (see Fig. 4). However, as the shear rate increases and the polymer melt enters the non-Newtonian area, θ stabilizes and becomes practically constant, thus no longer decreasing with rising shear rate. Fig. 4(a) shows that the θ of PMMA tends to stabilize when the shear rate reaches 1200 (1/s), reaching a value for θ in the region of 5.05–5.11 $\times 10^{-3}$. In Fig. 4(b), one can see the θ of COC stabilizes when the shear rate reaches 3000 (1/s), with its value ranging from 9.16 to 9.19 $\times 10^{-3}$. To simplify calculations, the average of the calculated values at steady state is used to determine the final equivalent pressure dependence parameter for θ. In the case of PMMA, the value is 5.07 $\times 10^{-3}$, while for COC, it is 9.17 $\times 10^{-3}$. Table 5 shows the D_3 for PMMA at 240 °C and COC at 260 °C, which is used in Eq. (7), as well as the other six Cross-WLF parameters.

When θ is stable, the outlet pressure P2 is depicted as a function of the difference in pressure data (see Fig. 4). Even at a constant shear rate, the differential pressure ΔP increases as the pressure within the cavity of the die rises. The current research reveals that increasing the pressure inside the capillary die causes the polymer melt to become more viscous, resulting in the weakening of the shear thinning process. The above conclusion can also be explained using the theory of molecular chain

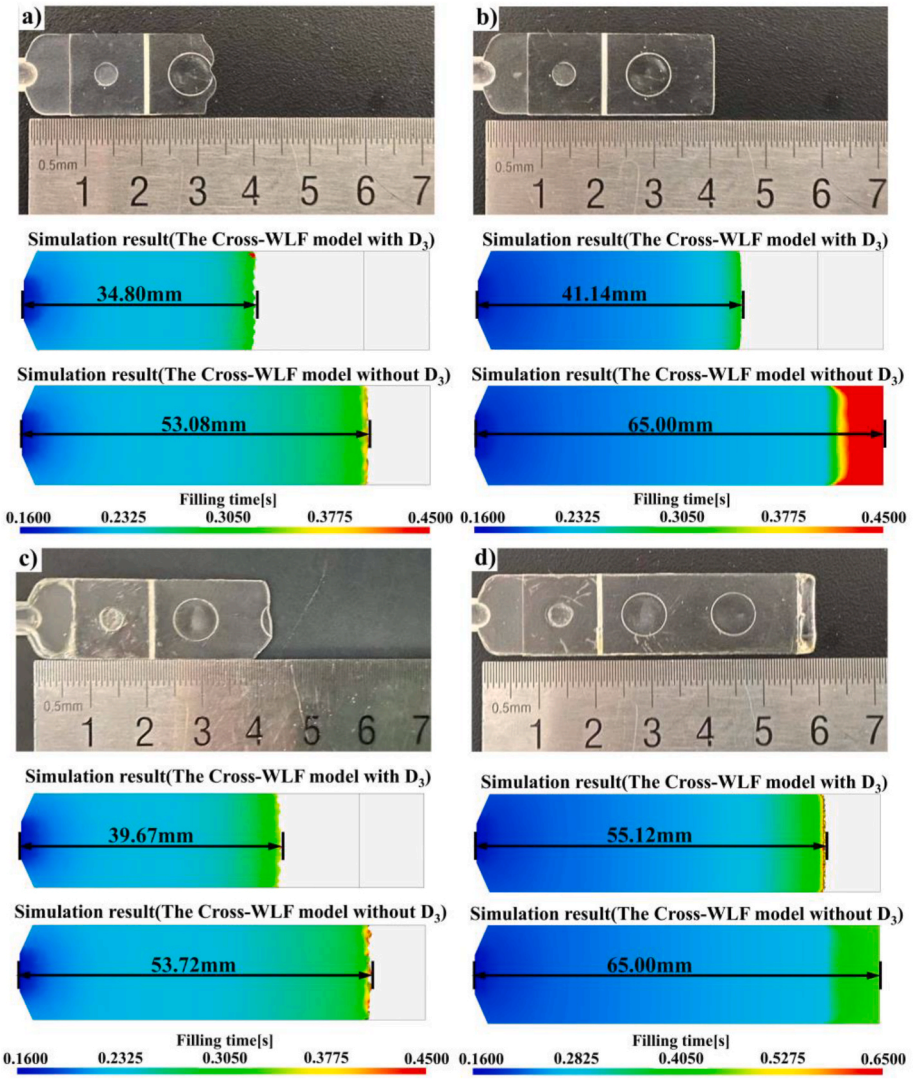

Fig. 8. Comparison of micro injection molding experiment and filling simulations of PMMA (a, b) for the 0.35 mm and 0.5 mm thin-walled model, and COC (c, d) for the 0.35 mm and 0.5 mm thin-walled model. Notice that in both cases the values of the filling simulation without D_3 is not in agreement with the experimental values.

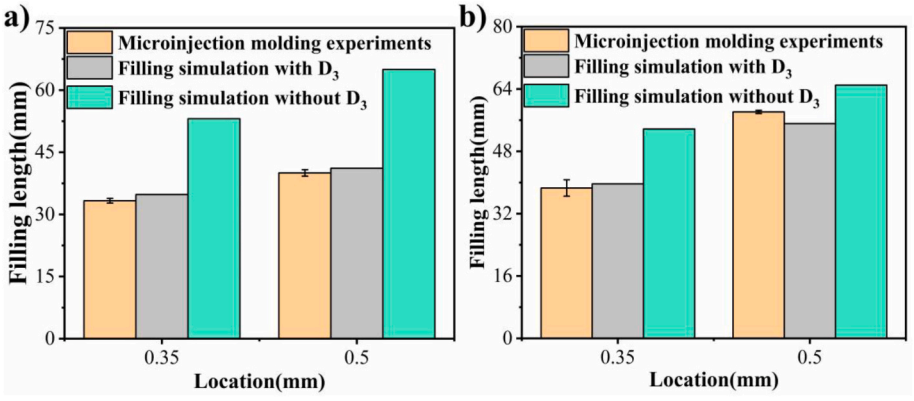

Fig. 9. Comparison of filling simulation results with microinjection molding experiment results for (a) PMMA, and (b) COC. Notice that in both cases the values of the filling simulation without D_3 is not in agreement with the experimental values.

disentanglement. When the counter pressure chamber is not installed, the outlet of the capillary tube is connected to the atmosphere. The outlet pressure is atmospheric and cannot be adjusted, while the molecular chains of the polymer are gradually disentangled under the action of shear stress, which reduces its viscosity and improves the fluidity. The outlet pressure can be adjusted via installing a counter pressure chamber at the outlet of the capillary, and increases analogously with the pressure difference inside the capillary die. The

Table 6
Error of micro injection molding experiment and simulation.

Materials	Model	Error between simulation and experimental results (with D_3)	Error between simulation and experimental results (without D_3)
PMMA (CM205)	0.35 mm thin-walled flat piece	3.90 ± 1.55 %	58.49 ± 2.37 %
	0.5 mm thin-walled flat piece	4.45 ± 1.04 %	62.61 ± 4.07 %
COC (5013L-10)	0.35 mm thin-walled flat piece	7.12 ± 1.56 %	37.54 ± 9.64 %
	0.5 mm thin-walled flat piece	4.96 ± 0.82 %	12.08 ± 0.97 %

Table 7
Process parameters set in the experiment and simulation and their specific values.

Materials	Process parameters	Value
PMMA (CM-205)	Injection rate	10 cm^3/s
	v/P switching pressure	80 MPa
	Mold temperature	80 °C
	Melt temperature	240 °C
	Holding pressure	80 MPa
	Holding time	5s
	Cooling time	30s
COC (5013L-10)	Injection rate	10 cm^3/s
	v/P switching pressure	80 MPa
	Mold temperature	100 °C
	Melt temperature	260 °C
	Holding pressure	80 MPa
	Holding time	5s
	Cooling time	30s

increased pressure difference leads to a re-entanglement of the molecular chain (to a certain degree). This entanglement is independent on the shear rate, the pressure-induced aggregation of molecular chains, as well as the pressure-sensitivity of the polymeric material. In micro injection molding, due to the fact that most of the molded parts are characterized by high aspect ratios and the presence of micro-structures, it is necessary to use great injection rate to complete the filling during the molding process. However, the large injection rate results in increased pressure in the mold cavity during injection, which makes the pressure sensitivity of polymers in micro injection molding a factor that should not be ignored.

3.3. Effect of pressure dependence parameter on simulation

In order to verify the accuracy of the Cross-WLF model that is containing D_3, the researchers conduct injection molding experiments using thin-walled parts with large width-to-thickness ratios (see Fig. 2) to directly compare with the simulation outcomes. The rheological properties of PMMA and COC are modified in Moldflow, and the Cross-WLF containing D_3 that is obtained using the experiment that is described in the previous section is put as input for the filling simulation. The original data in the Moldflow material library is utilized for the filling simulation under the same process parameters, which is then used for direct comparison. To better compare the experiment with the simulation, the samples need to be made short-shot. The range of process parameters that can short-shoot the slit model with different thicknesses was found through pre-experimentation, and the finalized process parameters are shown in Table 7. For each polymer material, ten stable injection molded samples will be selected for subsequent studies. The parameter settings of the molding experiments are identical to those of the filling simulations.

As can be seen in Fig. 5, regardless of the slit thickness (0.35 mm or 0.5 mm), the shear rate generated by filling simulations with the addition of D_3 is always smaller than the simulation results without it. Due to the high injection pressure used in the molding process, the shear rate of the polymer melt in the slit channel is reduced, weakening the shear thinning effect, thus making the polymer melt viscous, and preventing flow in the slit on its own. The distribution of the polymer flow front in the thin-walled region in Fig. 6 clearly supports the fillings of the preceding results. In the filling simulation without D_3, the flow front in the thin-walled region is sharper due to the significant shear interaction between the wall and the melt surface. In contrast, after adding D_3, the shear effect is reduced due to the pressure effect during the filling process. This results in a smoother melt flow front, and can be considered as proof that the pressure effect can reduce shear thinning. This conclusion is more intuitively drawn from the polymer shear viscosity data, which are extracted at the same time and position in Fig. 7. There, the viscosity obtained from the filling simulation with the addition of D_3 is evidently higher than the one obtained from the simulation without D_3. This fact is consistent with the concept noted in section 3.2, i.e. there is a thickening phenomenon of the pressure on the polymer melt during the flow under shear stress. As a result, the filling fails to successfully fill the cavity, leading to a short shot.

Comparing the experimental results with filling simulations using the same parameters, shows that the results of the filling simulations are closer to the experimental results after the addition of D_3 (see Fig. 8). Adding D_3 reduces errors in the filling simulation of PMMA and COC in thin-walled flat pieces(see Fig. 9).The accuracy of the filling simulation results with the inclusion of D_3 is significantly improved and the computational errors between the former and molded parts are less than 10 %, which is considered as an acceptable tolerance on many occasions in engineering (see Table 6).

The results prove that for the case of PMMA and COC, the filling simulation results of Cross-WLF for parts with large width-to-thickness ratios and with the addition of D_3 are much closer to the actual thin-walled parts obtained by injection molding, showcasing the huge importance of D_3 in micro injection molding simulation. When using CAE mold flow analysis to guide mold and part design, the polymer viscosity model must take into consideration the influence of the pressure dependence parameter on the filling process. If not, it will lead to short shots, warping, and other defects when performing the molding process. A comparison of simulation and experimental results also validates the reliability of the data calculations on D_3 in Section 3.2.

4. Conclusions

In this work, the shear viscosity and pressure dependence of PMMA and COC are characterized by capillary rheometer and counter pressure chamber. Furthermore, the pressure dependence parameter D_3 in the Cross-WLF model for describing polymer melt viscosity is characterized in the non-Newtonian region. The test results show that even if the shear rate remains constant during the test, the pressure difference between the two ends of the capillary die will increase. This results in the suppression of shear thinning of the polymer melt, i.e. the shear rate to which the polymer is subjected in the microchannel is reduced. This increases the viscosity of the polymer melt, making cavity filling more difficult. Short-shot filling simulation is performed using thin-walled parts with thickness of 0.35 and 0.5 mm. The same short-shot experiment is also done. It can be seen from the filling simulation that the flow front of the polymer melt containing D_3 in the Cross-WLF model becomes smoother under the same process parameter setting. This means that under the action of pressure, the wall shear of the polymer melt decreases and the polymer viscosity increases. This conclusion is also verified in simulated cloud images of shear viscosity and shear rate. The short-shot experiment are compared with the filling simulation. The

comparison shows that after adding D_3, the error between PMMA simulation and experiment is 3.90 ± 1.55 % and 4.45 ± 1.04 %. COC is 7.12 ± 1.56 % and 4.96 ± 0.82 %. This indicates that the filling simulation accuracy of microinjection molding has been greatly improved after adding D_3 to the Cross-WLF model. Therefore, the pressure dependence of the polymer needs to be considered in the mold design and filling simulation of micro injection molding.

This work aims to provide a richer perspective on filling simulation for micro injection molding and a better understanding of CAE simulation and design optimization prior to manufacturing micro injection molds.

CRediT authorship contribution statement

Junjie Liu: Writing – review & editing, Writing – original draft, Methodology. **Baishun Zhao:** Writing – review & editing, Conceptualization. **Dimitrios Kontziampasis:** Writing – review & editing, Visualization. **Bingyan Jiang:** Funding acquisition. **Wangqing Wu:** Software, Funding acquisition, Formal analysis.

Declaration of competing interest

The authors declare that they have no known competing financial interests or personal relationships that could have appeared to influence the work reported in this paper.

Data availability

Data will be made available on request.

Acknowledgements

The authors would like to acknowledge the financial support from the National Natural Science Foundation of China (Key International (Regional) Joint Research Program, [grant number 51920105008] and Normal project, [grant number 51875582] and the State Key Laboratory of Precision Manufacturing for Extreme Service Performance Program (No. ZZYJKT2023-11). The helpful comments of anonymous reviewers are gratefully acknowledged.

References

[1] R. Huang, X. Zhang, B.P. Ng, A.S. Kumar, K. Liu, Roll-to-Roll embossing of optical radial fresnel lenses on polymer film for concentrator photovoltaics: a feasibility study, Int. J. Precis. Eng. Manuf. Green Technol. 8 (2019) 1–12.
[2] L. Xirui, L. Chuang, Y. Chao, X. Changxi, Optimization of injection molding process parameters and axial surface compensation for producing an aspheric plastic lens with large diameter and center thickness, Appl. Opt. 58 (2019) 927–934.
[3] H.-Y. Zhang, N. Zhang, W. Han, H.-G. Zhang, M.D. Gilchrist, F.-Z. Fang, Characterization of process and machine dynamics on the precision replication of microlens arrays using microinjection moulding, Advances in Manufacturing 9 (2021) 1–23.
[4] M. Bricard, M. Guangrui, S. Zhijun, Y. Guang, Polymer-based microneedle composites for enhanced non-transdermal drug delivery, Appl. Mater. Today 29 (2022) 101659.
[5] Y.P. Ranjan, M.M. Nasrin, C. Lauryn, M. Golam, D. Lewis, S. Morayo, P.S. Kumar, U.M. Jasim, D.D. Bhusan, Translation of polymeric microneedles for treatment of human diseases: recent trends, progress, and challenges, Pharmaceutics 13 (2021) 1132, 1132.
[6] L.D. Pan, W.Q. Wu, J.J. Liu, X.P. Li, Ultrasonic plasticization microinjection precision molding of polypropylene microneedle arrays, ACS Appl. Polym. Mater. 5 (2023) 9354–9363.
[7] Y. Wenqian, G. Junfeng, L. Zheng, R. Shilun, C. Biaosong, S. Changyu, L.L. James, W. Xinyu, Study on the influence of microinjection molding processing parameters on replication quality of polylactic acid microneedle array product, Polymers 15 (2023) 1199, 1199.
[8] L. Binbin, W. Wangqing, H. Xiansong, L. Xuepeng, P. Lida, Z. Guangyan, Formation and prediction of the multi-layered crystalline structures in micro-injection molded small modulus gears, Polym. Test. 129 (2023) 108284.
[9] M. R., S. B.H., S.-N. K., A combined experimental-numerical approach for life analysis and modeling of polymer-based ternary nanocomposite gears, Tribol. Int. 173 (2022) 107654.
[10] L. Wang, Y. Zhang, L. Jiang, X. Yang, Y. Zhou, X. Wang, Q. Li, C. Shen, L.S. Turng, Effect of injection speed on the mechanical properties of isotactic polypropylene micro injection molded parts based on a nanoindentation test, J. Appl. Polym. Sci. 136 (2019) 47329.
[11] M. Heckele, W.K. Schomburg, Review on micro molding of thermoplastic polymers, J. Micromech. Microeng. 14 (2004) 1–14.
[12] G. J, C. T, M. P, Microinjection molding of thermoplastic polymers: a review, J. Micromech. Microeng. 17 (2007) 96–109.
[13] P. Deng, B. Whiteside, F. Wang, K. Norris, J. Zhang, Epitaxial growth and morphological characteristics of isotactic polypropylene/polyethylene blends: scale effect and mold temperature, Polym. Test. 34 (2014) 192–201.
[14] K.-Y. Jiang, J.-N. Tian, M.-J. Wang, J.-J. Ma, Z.-K. Yu, Influence of scale effect on filling behavior of injection molding by visualization method, Int. Polym. Process. 27 (2012) 25–29.
[15] L. Wang, Q. Li, W. Zhu, C. Shen, Scale effect on filling stage in micro-injection molding for thin slit cavities, Microsyst. Technol. 18 (2012) 2085–2091.
[16] L. Wang, L. Jiang, S. Li, Y. Zhang, D. Wang, Q. Li, C. Shen, Influence of scale effect and injection speed on morphology and structure of the microinjection molded isotactic polypropylene parts, Polym. Adv. Technol. 31 (2020) 1463–1473.
[17] C. Mnekbi, M. Vincent, J.F. Agassant, Polymer rheology at high shear rate for microinjection moulding, Int. J. Material Form. 3 (2010) 539–542.
[18] D. Z., K. S., Micro-injection molding of polymer nanocomposites composition-process-properties relationship, Int. Polym. Process. 36 (2021) 276–286.
[19] Q. Wang, C. Yang, K. Du, Z.H. Wu, Effect of micro injection molding parameters on cavity pressure and temperature assisted by Taguchi method, Mechanics 25 (2019) 261–268.
[20] H. Zhang, F. Fang, M.D. Gilchrist, N. Zhang, Filling of high aspect ratio micro features of a microfluidic flow cytometer chip using micro injection moulding, J. Micromech. Microeng. 28 (2018) 075005.
[21] G. Tosello, F.S. Costa, High precision validation of micro injection molding process simulations, J. Manuf. Process. 48 (2019) 236–248.
[22] G. Trotta, S. Cacace, Q. Semeraro, Optimizing process parameters in micro injection moulding considering the part weight and probability of flash formation, J. Manuf. Process. 79 (2022) 250–258.
[23] G. Gou, P. Xie, W. Yang, Y. Ding, Online measurement of rheological properties of polypropylene based on an injection molding machine to simulate the injection-molding process, Polym. Test. 30 (2011) 826–832.
[24] D.O. Kazmer, System identification and modeling of viscoelastic behavior from capillary melt rheological data, Polym. Eng. Sci. 54 (2014) 2824–2838.
[25] T. Sedlacek, M. Zatloukal, P. Filip, A. Boldizar, P. Saha, On the effect of pressure on the shear and elongational viscosities of polymer melts, Polym. Eng. Sci. 44 (2004) 1328–1337.
[26] T. Mattner, D. Drummer, Influence of pressure on end corrections in capillary rheometry, Rheol. Acta 55 (2016) 823–832.
[27] M. Evan, G.H. S, Rheological properties related to extrusion of polyolefins, Polymers 13 (2021) 489.
[28] R. Cardinaels, P. Puyvelde, P. Moldenaers, Evaluation and comparison of routes to obtain pressure coefficients from high-pressure capillary rheometry data, Rheol. Acta 46 (2007) 495–505.
[29] M. Dees, M. Mangnus, N. Hermans, W. Thaens, A.-S. Hanot, P.V. Puyvelde, On the pressure correction of capillary melt rheology data, Rheol. Acta 50 (2011) 117–124.
[30] R. Carl, T. Richard, M. Tom, Pressure and shear rate dependence of the viscosity and stress relaxation of polymer melts, J. Rheol. 62 (2018) 631–642.
[31] H. Münstedt, Influence of hydrostatic pressure on rheological properties of polymer melts—a review, J. Rheol. 64 (2020) 751–774.
[32] V. Volpe, R. Pantani, Determination of the effect of pressure on viscosity at high shear rates by using an injection molding machine, J. Appl. Polym. Sci. 135 (2018) 45277.
[33] S. Raha, H. Sharma, M. Senthilmurugan, S. Bandyopadhyay, P. Mukhopadhyay, Determination of the pressure dependence of polymer melt viscosity using a combination of oscillatory and capillary rheometer, Polym. Eng. Sci. 60 (2020) 517–523.
[34] S. Sandra, S. Alankar, C. Camilo, R. Gilles, A. Amine, Towards an accurate pressure estimation in injection molding simulation using surrogate modeling, Int. J. Material Form. 15 (2022) 72.
[35] E.S. Carreras, N.E. Kissi, J.-M. Piau, F. Toussaint, S. Nigen, Pressure effects on viscosity and flow stability of polyethylene melts during extrusion, Rheol. Acta 45 (2006) 209–222.
[36] J. Aho, S. Syrjälä, Measurement of the pressure dependence of viscosity of polymer melts using a back pressure-regulated capillary rheometer, J. Appl. Polym. Sci. 117 (2010) 1076–1084.
[37] P.V. Puyvelde, A. Vananroye, A.-S. Hanoi, On the pressure dependency of the Bagley correction, Int. Polym. Process.: J. Polym. Process. Soc. 28 (2013) 558–564.
[38] Z.Y. Wang, Y.C. Lam, X. Chen, S.C. Joshi, Viscosity corrections for concentrated suspension in capillary flow with wall slip, AIChE J. 56 (2010) 1447–1455.